

# Tensor network study of the spin-1/2 square-lattice $J_1$ - $J_2$ - $J_3$ model: incommensurate spiral order, mixed valence-bond solids, and multicritical points

Wen-Yuan Liu,<sup>1</sup> Didier Poilblanc,<sup>2</sup> Shou-Shu Gong,<sup>3</sup> Wei-Qiang Chen,<sup>4,5</sup> and Zheng-Cheng Gu<sup>6</sup>

<sup>1</sup>*Division of Chemistry and Chemical Engineering, California Institute of Technology, Pasadena, California 91125, USA*

<sup>2</sup>*Laboratoire de Physique Théorique, C.N.R.S. and Université de Toulouse, 31062 Toulouse, France*

<sup>3</sup>*School of Physical Sciences, Great Bay University, Dongguan 523000, China, and  
Great Bay Institute for Advanced Study, Dongguan 523000, China*

<sup>4</sup>*Shenzhen Institute for Quantum Science and Engineering and Department of Physics,  
Southern University of Science and Technology, Shenzhen 518055, China*

<sup>5</sup>*Shenzhen Key Laboratory of Advanced Quantum Functional Materials and Devices,  
Southern University of Science and Technology, Shenzhen 518055, China*

<sup>6</sup>*Department of Physics, The Chinese University of Hong Kong, Shatin, New Territories, Hong Kong, China*

(Dated: September 26, 2023)

We use the finite projected entangled pair state (PEPS) method to investigate the global phase diagram of the spin-1/2 square-lattice  $J_1$ - $J_2$ - $J_3$  antiferromagnetic (AFM) Heisenberg model. The ground state phase diagram is established with a rich variety of phases: AFM, gapless quantum spin liquid, valence-bond solid (VBS), stripe, and incommensurate spiral phases. The nature of the VBS region is revealed, containing a plaquette VBS and a mixed columnar-plaquette VBS, with the emergence of short-range incommensurate spin correlations in some region. The long-range incommensurate magnetic phase is also explicitly characterized as a planar spiral with incommensurate spatial periodicities. Most interestingly, there exists several multicritical points connecting different phases. These findings elucidate the true nature of the long-standing square-lattice  $J_1$ - $J_2$ - $J_3$  antiferromagnet at zero-temperature. Our results also pave the way to accurately simulate complex two-dimensional quantum systems that may host nonuniform features by means of finite PEPS.

## I. INTRODUCTION

The spin-1/2  $J_1$ - $J_2$ - $J_3$  antiferromagnetic (AFM) Heisenberg model on a square lattice is one of the paradigmatic prototypes to study frustrated magnets. This model has attracted a lot of interest after the application of Anderson's resonating valence-bond (RVB) theory to high-temperature superconductors [1]. The Hamiltonian is described as follows:

$$H = J_1 \sum_{\langle i,j \rangle} \mathbf{S}_i \cdot \mathbf{S}_j + J_2 \sum_{\langle\langle i,j \rangle\rangle} \mathbf{S}_i \cdot \mathbf{S}_j + J_3 \sum_{\langle\langle\langle i,j \rangle\rangle\rangle} \mathbf{S}_i \cdot \mathbf{S}_j, \quad (1)$$

where  $J_1$ ,  $J_2$ ,  $J_3$  denotes the first-, second- and third-nearest neighbour couplings, and the summations run over all corresponding spin pairs. For positive  $J_i$ , the three kinds of interactions compete each other, leading to intractable difficulties for analytic and numerical studies. The classical phase diagram given by spin-wave theory contains four phases: (i) an AFM phase ordered at wave vector  $\mathbf{k}_0 = (\pi, \pi)$ , (ii) a stripe phase ordered at wave vector  $\mathbf{k}_x = (\pi, 0)$  or  $\mathbf{k}_y = (0, \pi)$ , (iii) a spiral phase at  $\mathbf{Q}_x = (\pm q, \pi)$  or  $\mathbf{Q}_y = (\pi, \pm q)$  with  $\cos q = (2J_2 - J_1)/4J_3$ , and (iv) another spiral phase at  $\mathbf{Q} = (\pm q, \pm q)$  with  $\cos q = -J_1/(2J_2 + 4J_3)$  [2, 3]. The AFM and the spiral  $(\pm q, \pm q)$  phases are separated by a classical critical line  $(J_2 + 2J_3) = J_1/2$ . However, the quantum phase diagram with spin-1/2 is still unclear.

It is well accepted that at small  $J_2$  and  $J_3$ , the model possesses AFM order [3–6]. At large  $J_2$  and  $J_3$ , the corresponding stripe and spiral orders will develop [7]. The controversy focuses on the intermediate region of  $J_2$  and  $J_3$ , especially along the classical critical line. Some theories strongly suggest that the combined effect of quantum fluctuations and frustration is strong enough to destroy the long-range orders and stabilize

paramagnetic states along the critical line, including spin-wave theories [3, 4, 6], the renormalization group (RG) analysis of the non-linear  $\sigma$  model [8], series expansions [2], a momentum-shell RG calculation [9], etc. There are also other theories supporting the existence of paramagnetic states but for  $J_2$  and  $J_3$  shifted to larger values with respect to the classical critical line by quantum fluctuations [7, 10].

From the combined analyses of different studies, it seems most likely there exists an intermediate nonmagnetic region. Nevertheless, the nature of the nonmagnetic region is also far from clear. Large- $N$  results and series expansions predict that this intermediate state is spontaneously dimerized [2, 7], while spin-wave theory predicts that this intermediate state is a spin liquid [3, 4, 6]. For the pure  $J_1$ - $J_3$  model, i.e., the  $J_2 = 0$  case, a Monte Carlo study of the classical limit supplemented by analytical arguments on the role of quantum fluctuations supports the emergence of VBS or  $Z_2$  spin liquid phases between the AFM and spiral phases [11]. Exact diagonalizations of periodic clusters suggest a VBS state with incommensurate short-range correlations [12], but the density matrix renormalization group (DMRG) results are consistent with a gapped spin liquid [13]. For  $J_2 \neq 0$ , a short-range valence bond study finds a plaquette VBS state along the line  $J_2 + J_3 = J_1/2$  (where the description in terms of nearest-neighbor singlet coverings is excellent) [14]. Later, a mixed columnar-plaquette VBS state [15] was proposed which possesses long-range plaquette order but breaks isotropy between  $x$ - and  $y$ - directions, supporting the findings in a previous approach [16]. Also, exact diagonalizations [17] showed that quantum fluctuations could lead to new quantum phases.

The special case of the  $J_1$ - $J_2$ - $J_3$  model with  $J_3 = 0$ , i.e., the  $J_1$ - $J_2$  model, is of great interest in the field of quantum magnets, which has been intensively studied for more than

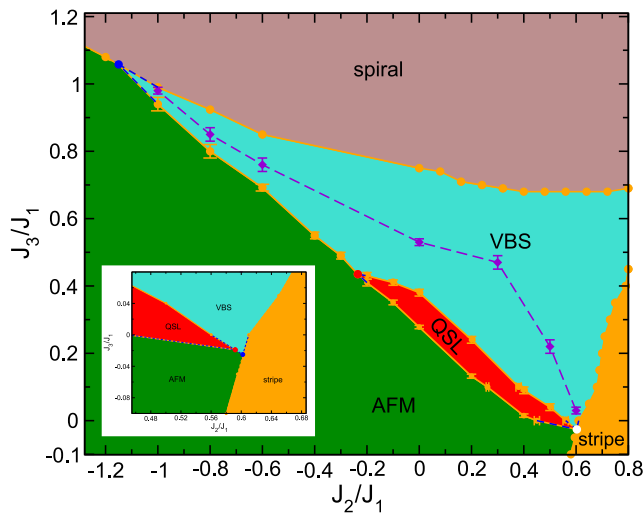


Figure 1. Ground state phase diagram of the spin-1/2 square-lattice  $J_1$ - $J_2$ - $J_3$  AFM model: the AFM phase ordered at  $(\pi, \pi)$ , the stripe phase ordered at  $(0, \pi)$  or  $(\pi, 0)$ , the spiral phase ordered at  $(\pm q, \pm q)$ , the gapless QSL phase (red) and the VBS phase. In the VBS region, below the violet dashed line is a plaquette VBS and above is a mixed columnar-plaquette VBS. Tricritical points (end points) are shown by red (blue) dots. The AFM-spiral, AFM-stripe, VBS-spiral and VBS-stripe transitions are first-order, and other phase transitions are continuous. The region in the right corner might contain a quadruple point (the white dot) connecting the VBS, QSL, AFM and stripe phases, or two multicritical points shown in the inset (assuming the gapless QSL does not touch the stripe phase).

three decades. The  $J_1$ - $J_2$  model exhibits an AFM phase in the region  $0 \leq J_2/J_1 \leq 0.45$  and a stripe phase for  $J_2/J_1 \geq 0.61$ . The intermediate nonmagnetic region has been investigated with many different methods [4, 5, 14, 18–60] and the existence of two successive gapless quantum spin liquid (QSL) and VBS phases lying between the AFM and stripe phases is being supported by more recent works [53, 58–60]. In particular, the finite PEPS method provides very solid results and makes it possible to extract critical exponents to understand the physical nature of the AFM-QSL and QSL-VBS transitions [59], indicating an intrinsic relation between the gapless QSL and the deconfined quantum critical point (DQCP) [61].

Very recently, a tensor network study has also revealed exotic properties in the  $J_1$ - $J_2$ - $J_3$  model [62]. Specifically, highly accurate tensor network results from finite and infinite PEPS methods, not only confirm the existence of QSL and VBS phases in the  $J_1$ - $J_2$  model, but even demonstrates the intrinsic relation between the gapless QSL and the DQCP, offering a fantastic scenario to understand the two exotic quantum phenomena. The existence of QSL and VBS phases in the pure  $J_1$ - $J_3$  model, i.e.,  $J_2 = 0$ , is also supported by recent DMRG calculations [63].

However, because of the highly complex competition of  $J_1$ ,  $J_2$  and  $J_3$  interactions, the global phase diagram of the  $J_1$ - $J_2$ - $J_3$  model remains enigmatic, particularly in regions which may involve nonuniform physical properties like incommen-

surate spin correlations. Thanks to the advancement of tensor network methods, we can now study this model in a precise way. One approach to study this model is based on the widely used infinite PEPS (iPEPS) ansatz [62]. Although it has a presumed unit cell, the nonuniform properties can still be investigated by systematically enlarging the unit cell. There have been remarkable progresses in correlated electron models [64–66]. In this paper, we shed new light on the ground state phase diagram of the  $J_1$ - $J_2$ - $J_3$  model by using an alternative approach, namely, the finite PEPS ansatz, which is well-suited for describing nonuniform features with site-independent tensors. Finite PEPS work very well in the scheme combined with variational Monte Carlo, and full details of the algorithm can be found in preceding publications [59, 62, 67, 68]. The obtained phase diagram is presented in Fig. 1.

Rest of the paper is organized as follows. In Sec. II, we first present results obtained for  $J_2 = 0$ . By computing spin and dimer order parameters, as well as ground state energies, we provide a complete phase diagram of the  $J_1$ - $J_3$  model, and focus on the emergence of incommensurate spiral spin correlations upon increasing  $J_3$ . Then, we consider an intermediate  $J_2 \neq 0$  term to further analyze the properties of the VBS phase. Next we consider a large enough negative  $J_2$  which suppresses the intermediate VBS phase, and eventually leads to a direct first-order AFM-spiral phase transition. Finally, we consider the  $J_3 < 0$  case to obtain the complete phase diagram, where the gapless QSL and VBS phases eventually disappear and a direct AFM-stripe transition occurs. In Sec. III, we discuss the existing results and obtain a refined description of the phase diagram of the  $J_1$ - $J_2$ - $J_3$  model. Finally, three appendices on the convergence with bond dimension, on ED on a small periodic  $4 \times 4$  cluster and on a refined analysis of the spin structure factor in the mixed VBS phase are provided.

## II. RESULTS

We use the recently developed finite PEPS method to perform all the calculations [67, 68]. The finite PEPS method works very well in the scheme of variational Monte Carlo approach, where the summation of physical degrees of freedom is replaced by Monte Carlo sampling, and thus one only needs to deal with single-layer tensor networks with a computational cost scaling  $O(D^6)$  where  $D$  is the tensor bond dimension. Such an approach has been successfully applied to solve very challenging quantum many-body problems [59, 62, 69, 70]. Previously, we have demonstrated that  $D = 8$  can produce well converged results for the  $J_1$ - $J_2$ - $J_3$  model up to  $20 \times 28$  sites [62]. Here we have again checked the  $D$ -convergence on an open  $16 \times 16$  cluster at  $(J_2, J_3) = (-1, 0.8)$  and find that  $D = 8$  indeed produces converged energy and order parameters, as shown in Appendix A. Therefore, we just use  $D = 8$  for all calculations and we set  $J_1 = 1$  unless otherwise specified.

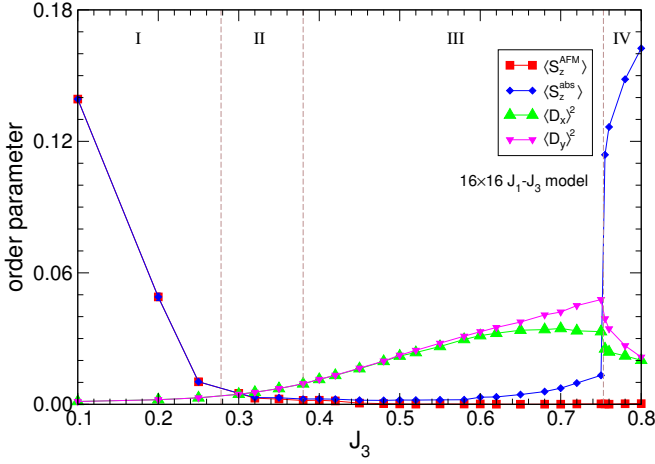


Figure 2. Variation of the local order parameters with respect to  $J_3/J_1$  on a  $16 \times 16$  system, including  $\langle S_z^{\text{AFM}} \rangle$ ,  $\langle S_z^{\text{abs}} \rangle$  and  $\langle D_x \rangle^2$  and  $\langle D_y \rangle^2$ . Phase boundaries between the different AFM (I), QSL (II), VBS (III) and spiral (IV) phases are denoted by vertical dashed lines, located at  $J_3 = 0.28, 0.38$  and  $0.752$ , respectively.

### A. $J_2 = 0$

#### 1. Order parameters

Through detailed computations, we find four phases by varying  $J_3$ : (I) the AFM phase ordered at  $\mathbf{k}_0 = (\pi, \pi)$ , (II) the gapless QSL phase, (III) the VBS phase, and (IV) the long-range spiral ordered phase. These four phases have been displayed in Fig. 2 along the  $J_3$  axis. Note that, when  $J_3$  is sufficiently large, phase (IV) evolves continuously to a (commensurate) spiral phase ordered at  $\mathbf{k}_1 = (\pm\pi/2, \pm\pi/2)$  which we label as phase (V).

The gapless spin liquid phase and the associated AFM-QSL and QSL-VBS phase transitions have been studied in a previous paper [62]. Now we consider the VBS-spiral transition. We define two local order parameters to detect long-range spin ordered phases:

$$\langle S_z^{\text{abs}} \rangle = \frac{1}{L^2} \sum_{i_x, i_y} |\langle S_{i_x, i_y}^z \rangle| \quad (2)$$

$$\langle S_z^{\text{AFM}} \rangle = \frac{1}{L^2} \sum_{i_x, i_y} (-1)^{i_x + i_y} \langle S_{i_x, i_y}^z \rangle \quad (3)$$

Since  $\langle S_z^{\text{abs}} \rangle$  is the average of the absolute value of the onsite  $\langle S_{i_x, i_y}^z \rangle$ , it can distinguish magnetic phases from nonmagnetic ones. Note  $\langle S_z^{\text{AFM}} \rangle$  is the standard AFM order parameter, which can distinguish the AFM phase from other phases including magnetic ones. These two order parameters should be zero theoretically on finite systems because of the SU(2) symmetry, but it is expected that for magnetic phases the corresponding ground state may break SU(2) symmetry and show nonzero values for  $\langle S_z^{\text{abs}} \rangle$  or  $\langle S_{i_x, i_y}^z \rangle$ , if system size is large enough.

In Fig. 2, we show the variation of  $\langle S_z^{\text{abs}} \rangle$  and  $\langle S_z^{\text{AFM}} \rangle$  with increasing  $J_3$  on  $16 \times 16$  systems. Indeed, in the AFM phase,

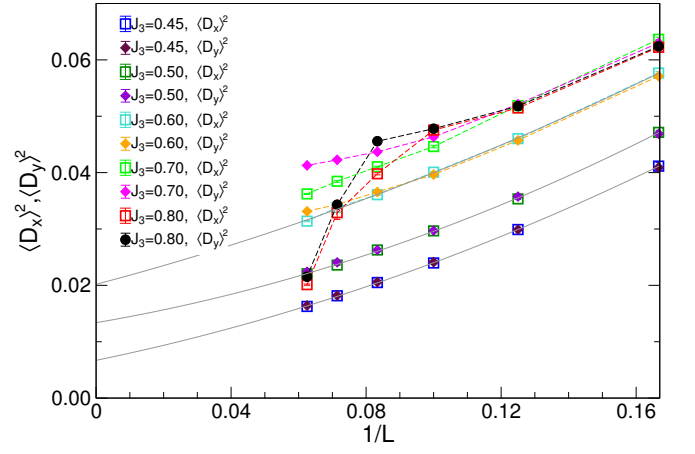


Figure 3. Dimer orders along  $x$ - and  $y$ - directions on  $L \times L$  systems with  $L = 6 - 16$  at different  $J_3$  using a fixed  $J_2 = 0$ . Solid gray lines denote second order polynomial fits for  $\langle D_x \rangle^2$  at  $J_3 = 0.45, 0.50$  and  $0.60$ .

$\langle S_z^{\text{abs}} \rangle$  and  $\langle S_z^{\text{AFM}} \rangle$  are equal and finite. After entering into the nonmagnetic QSL and VBS phases, SU(2) symmetry is almost restored completely, signaled by much smaller values of  $\langle S_z^{\text{abs}} \rangle$  and  $\langle S_z^{\text{AFM}} \rangle$  close to zero. When approaching the spiral phase, SU(2) symmetry is broken again and  $\langle S_z^{\text{abs}} \rangle$  gets very quickly significantly larger, indicating a first-order phase transition to a magnetic phase at  $J_3 \approx 0.75$ . In addition, we observe that  $\langle S_z^{\text{AFM}} \rangle$  still vanishes, which actually is the result of an incommensurate spin pattern.

#### 2. Nature of the VBS phase

We also check the dimer order parameters, defined as [59]

$$D_\alpha = \frac{1}{N_b} \sum_{\mathbf{i}} (-1)^{i_\alpha} B_{\mathbf{i}}^\alpha, \quad (4)$$

where  $B_{\mathbf{i}}^\alpha = \mathbf{S}_{\mathbf{i}} \cdot \mathbf{S}_{\mathbf{i} + \mathbf{e}_\alpha}$  is the bond operator between site  $\mathbf{i}$  and site  $\mathbf{i} + \mathbf{e}_\alpha$  along  $\alpha$  direction with  $\alpha = x$  or  $y$ .  $N_b = L(L-1)$  is the total number of counted bonds. As seen in Fig. 2, from the VBS phase to the spiral phase, the VBS order parameters  $\langle D_x \rangle^2$  and  $\langle D_y \rangle^2$  also show sudden changes, consistent with a first-order phase transition scenario.

We observe that  $\langle D_x \rangle^2$  and  $\langle D_y \rangle^2$  are equal for  $J_3 < 0.55$  and their difference increases when  $J_3$  is beyond  $0.55$ . We believe that the difference between  $\langle D_x \rangle^2$  and  $\langle D_y \rangle^2$  might be induced by short-range spiral correlations (SRSC). By analyzing the spin-spin correlations, we see that SRSC appear already for  $J_3 = 0.45$ . This suggests that strong enough SRSC at  $J_3 \approx 0.55$  may induce different VBS order parameters  $\langle D_x \rangle^2$  and  $\langle D_y \rangle^2$ , which is a characteristic feature of the mixed-VBS phase.

In Fig. 3, we present the dimer orders  $\langle D_x \rangle^2$  and  $\langle D_y \rangle^2$  with respect to  $1/L$ . Here we do not show all the finite-size scaling extrapolations for clarity, but we can clearly see that at  $J_2 = 0.8$  the dimer orders will vanish in the thermodynamic limit.

In the VBS region  $0.37 < J_3 \lesssim 0.75$  with  $J_3 = 0.45$  and  $0.50$ , the extrapolated  $\langle D_x \rangle^2$  and  $\langle D_y \rangle^2$  values in the thermodynamic limit seem to be identical, corresponding to the plaquette VBS order. At  $J_3 = 0.60$  and  $0.70$ , the extrapolated values of  $\langle D_x \rangle^2$  and  $\langle D_y \rangle^2$  are different and nonzero, excluding a plaquette VBS phase and indicating a mixed columnar-plaquette VBS. Of course, we can not completely exclude a pure columnar phase due to the limitation of system sizes.

We note that exact diagonalizations up to 32 sites with twisted boundary conditions, mark the region  $0.5 \lesssim J_3 \lesssim 0.57$  as a mixed columnar-plaquette VBS, then followed by a SRSC state before entering the long-range spiral ordered phase [17]. This is roughly consistent with our results, but the SRSC state revealed by the ED result is actually part of the VBS phase. In addition, a short-range valence bond study suggests a plaquette VBS state along the line  $J_2 + J_3 = J_1/2$  [14]. In combination with our results, this suggests that the VBS phase is most likely comprised of a plaquette and a mixed columnar-plaquette phase, and the transition between them is continuous. A similar scenario has been reported in a quantum dimer model on square lattices, where a mixed columnar-plaquette VBS phase continuously intervenes between columnar and plaquette VBS phases [71]. Qualitatively, we know that competition between  $J_1$  and  $J_3$  couplings tends to induce spiral orders. However, when  $J_3$  is too small to lead to SRSC, the isotropy between the  $x$ - and  $y$ - directions survives, consistently with the existence of a plaquette VBS phase. When  $J_3$  gets larger, rotation symmetry spontaneously breaks down giving rise to a mixed columnar-plaquette VBS phase.

### 3. Energy curve versus $J_3$

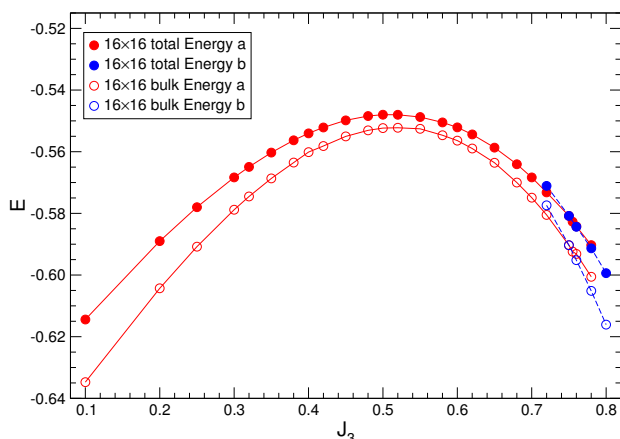


Figure 4. Ground state energy per site at different  $J_3$  ( $J_1 = 1$  and  $J_2 = 0$ ) on a  $L \times L$  ( $L = 16$ ) open system using the full cluster (filled circle) or only the central  $(L-8) \times (L-8)$  bulk region (unfilled circle). For the cases of  $J_3 > 0.65$  (red symbols), we use the ground state with a slightly smaller  $J_3$  as an initialization for optimization. As a comparison, we also use the ground state with  $J_3 = 0.8$  as an initialization for optimization (blue symbols). Thanks to hysteresis, the first-order phase transition point can be located by their crossing.

To have a much more comprehensive understanding of various phases, we also consider how the energy changes with respect to  $J_3$ . In Fig. 4, we plot the energy per site at different  $J_3$  based on  $16 \times 16$  sites. The filled circles (red and blue) denote the energy per site from the full systems, and the unfilled ones (red and blue) are correspondingly energy per site from the central  $8 \times 8$  bulk. We can see that the energy of the  $16 \times 16$  system has a maximum around  $J_3 \approx 0.52$ . Interestingly, this point corresponds to the expectation value of the third-nearest neighbour interaction terms changing sign. However, the first-order transition does not occur at this point, the energy changing smoothly in its neighborhood. The first-order transition point indeed occurs at  $J_3 > 0.7$ . To locate the transition point from the ground state energy curve, we first use the ground state at  $J_3 = 0.65$  (with initialization by simple update [72]), as an initialization for further optimization to obtain the ground state at  $J_3 = 0.68$ , and then use the state at  $J_3 = 0.68$  to get the optimized state at  $J_3 = 0.70$ , and further on to get the optimized states of  $J_3 = 0.72, 0.75$  and  $0.78$  sequentially. Such a process can be viewed as an adiabatic evolution process. We can also complete the reverse process starting from the ground state at  $J_3 = 0.80$  moving backwards to sequentially get the optimized states at  $J_3 = 0.78, 0.755, 0.75$  and  $0.72$ , respectively. Except in rare special cases, first-order transitions generically show hysteresis under such an evolution i.e. one does not transit spontaneously between the two phases. The transition point can then be obtained from the crossing of the energy curves of the two evolution paths. In Fig. 4, we can see that the whole energy per site of the  $L \times L$  ( $L = 16$ ) system (solid red and blue circles) obtained from the two different paths showing a crossing around  $J_3 \approx 0.75$ . We can see the crossing even more clearly from the energy of the central  $(L-8) \times (L-8)$  bulk region which provides a better estimate of the energy in the thermodynamic limit. Both analyses indicate the VBS-spiral transition occurs at  $J_3 \approx 0.75$ , in good agreement with the behaviour of the spin order parameter  $\langle S_z^{\text{abs}} \rangle$  which shows an apparent discontinuity at the same  $J_3$  value, as shown in Fig. 2. We note the VBS-spiral transition point can even be estimated via the second derivative of the energy with respect to  $J_3$  on a periodic  $4 \times 4$  cluster, providing identical results, as shown in Appendix B.

### 4. Incommensurate spiral order

Now we see how spiral order evolves with increasing  $J_3$ , focusing on the  $J_1$ - $J_3$  model, by computing the spin structure factor defined as

$$S(\mathbf{k}) = \frac{1}{L^2} \sum_{ij} \langle \mathbf{S}_i \cdot \mathbf{S}_j \rangle e^{i\mathbf{k} \cdot (\mathbf{i}-\mathbf{j})}. \quad (5)$$

We compute all pairs of spin correlators  $\langle \mathbf{S}_i \cdot \mathbf{S}_j \rangle$  to get the structure factor. In the classical  $J_1$ - $J_3$  model, for  $J_3 \leq 0.25$ , the ground state is a conventional AFM phase with magnetic wave vector  $\mathbf{k}_0 = (\pi, \pi)$ . For  $J_3/J_1 > 0.25$ , the ground state has planar incommensurate magnetic order at a wave vector  $\mathbf{Q} = (\pm q, \pm q)$ . With  $J_3/J_1$  increasing, the spiral order is incommensurate except at  $J_3/J_1 = 0.5$  and  $J_3/J_1 \rightarrow \infty$ , and

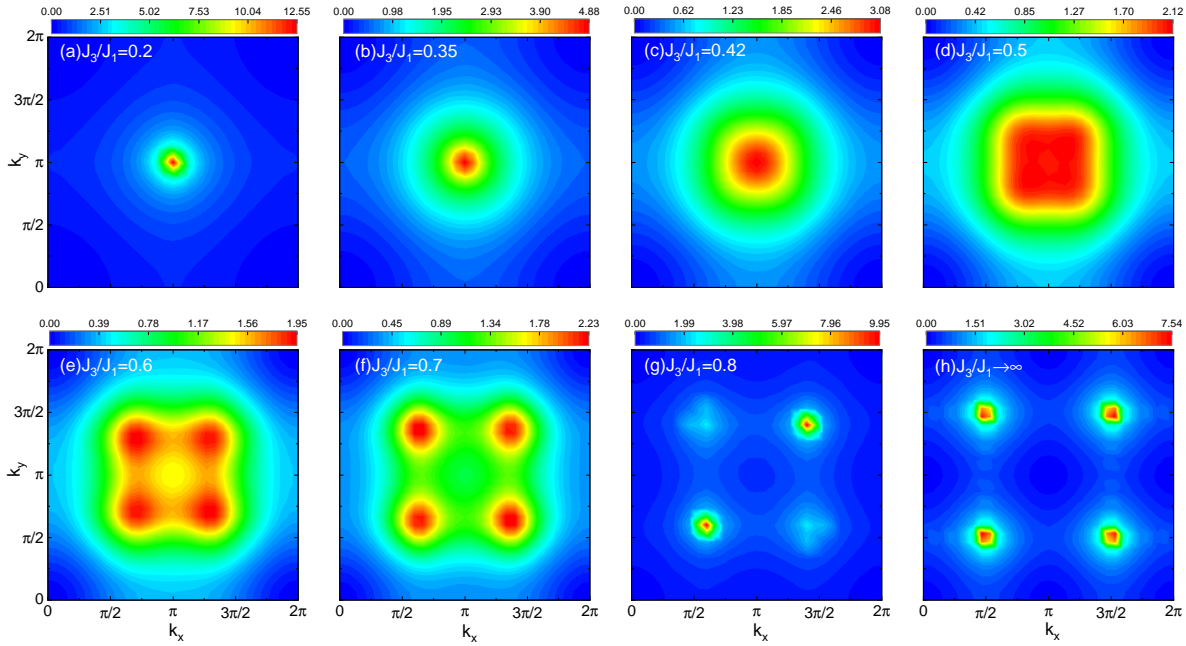


Figure 5. Given  $J_2 = 0$ , evolution of the spin structure factor with increasing  $J_3/J_1$  on  $16 \times 16$  sites (a)-(h). (a)  $J_3/J_1 = 0.2$  is in the AFM phase; (b)  $J_3/J_1 = 0.35$  is in the gapless QSL phase; (c)-(f)  $J_3/J_1 = 0.42, 0.5, 0.6, 0.7$  are in the VBS phase; (g)  $J_3/J_1 = 0.8$  is an incommensurate spiral phase with magnetic Bragg peaks at  $(q, q)$  and  $(-q, -q)$  where  $q \approx \frac{3}{5}\pi$ ; (h)  $J_3/J_1 \rightarrow \infty$  is a  $S(\pi/2, \pi/2)$  phase.

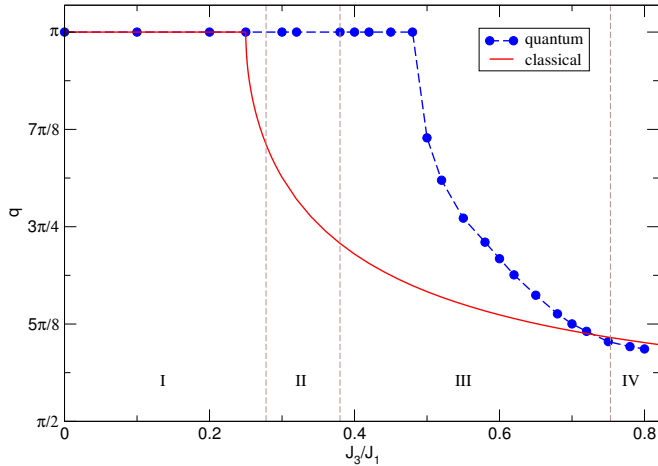


Figure 6. Variation of the peak position  $\mathbf{Q} = (q, q)$  in the spin structure factor  $S(\mathbf{k})$ . Blue symbols represent the peak position obtained in the spin-1/2  $J_1$ - $J_3$  model on a  $16 \times 16$  cluster. Red lines denote the peak position from the classical  $J_1$ - $J_3$  model. Vertical dashed lines separate the four phases in the quantum case: (I) AFM, (II) QSL, (III) VBS and (IV) spiral phases.

the wave vector  $\mathbf{Q} = (\pm q, \pm q)$  will gradually move from  $q = \pi$  to  $q = \pi/2$  according to the formula  $q = \cos^{-1}(-0.25J_1/J_3)$  for  $J_3/J_1 > 0.25$  [11, 73].

In Fig. 5(a)-(h), we show the spin structure factor of spin-1/2  $16 \times 16$  sites for different  $J_3$  at a fixed  $J_2 = 0$ . At  $J_3 = 0.2$  (in AFM phase),  $0.35$  (in QSL phase) and  $0.42$  (in VBS phase), the peaks of the spin structure factor are located at  $\mathbf{k}_0 = (\pi, \pi)$ . Further increasing  $J_3$ , the peak will

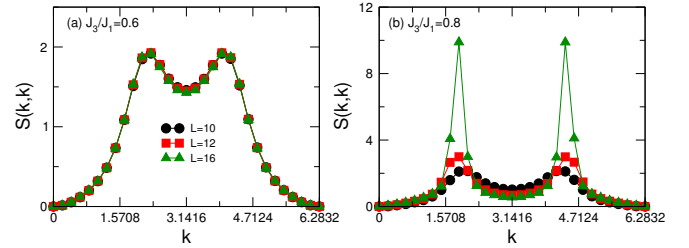


Figure 7. Variation with system size  $L$  of the spin structure factor in the  $J_1 - J_3$  model at  $J_3 = 0.6$  and  $0.8$ .  $S(\mathbf{k}) = S(k_x, k_y)$  is shown along the  $k_x = k_y$  line for simplicity. Clear magnetic Bragg peaks are developing at  $J_3 = 0.8$ , in contrast to  $J_3 = 0.6$ .

gradually move from  $\mathbf{k}_0 = (\pi, \pi)$  to  $\mathbf{Q} = (\pm q, \pm q)$ . If  $J_3/J_1 \rightarrow \infty$  (set  $J_1 = 0$ ), the magnetic order will approach to  $\mathbf{Q} = (\pm\pi/2, \pm\pi/2)$ , as shown in Fig. 5(h). In Fig. 6, we present the classical and quantum results for a clear comparison. We would like to mention that a careful inspection of the data of Fig. 5(f) reveals a detectable difference in the magnitudes of the maxima (see Appendix C), indeed expected in the mixed VBS phase breaking  $\pi/2$ -rotation.

We point out that we found (short-range) incommensurate spin correlations at  $J_3 = 0.45$  in the VBS phase, but long-range spiral order is truly established for  $J_3 > 0.75$ , as we have discussed in the previous part. The spiral order parameter in the VBS phase is short-ranged as it scales to zero in the thermodynamic limit. As shown in Fig. 7, with increasing of system size  $L$ , the peak value of the structure factor at  $J_3 = 0.6$  almost stays constant, indicating a vanishing spin order. In contrast, at  $J_3 = 0.8$  the peak value diverges quickly,

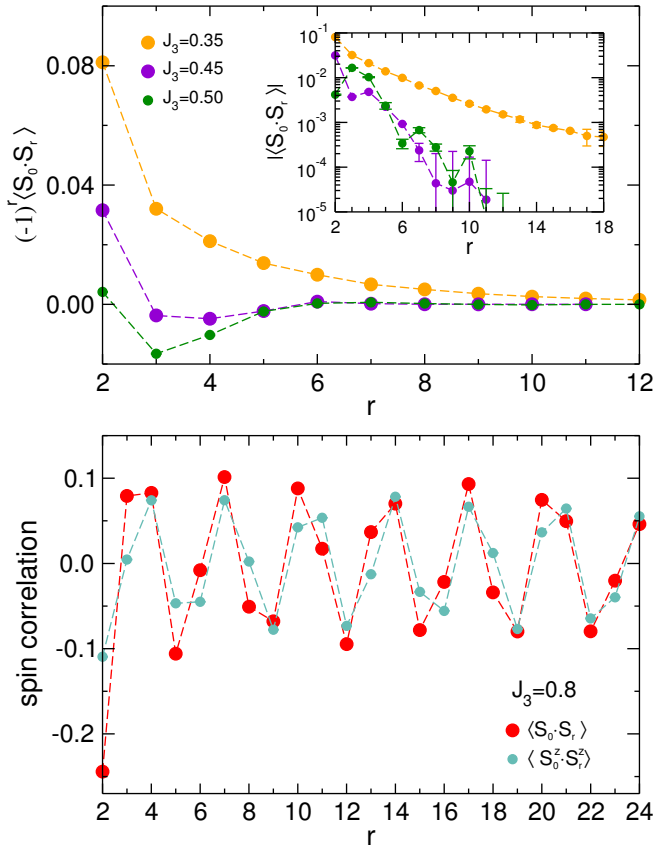


Figure 8. Spin-spin correlations along the central line  $y = L_y/2$  on long strips  $L_y \times L_x$  with  $L_x = 28$  for the  $J_1$ - $J_3$  model. Upper panel: correlations at  $J_3 = 0.45, 0.50$  (exponential decay) on  $L_y = 12$ , compared to  $J_3 = 0.35$  on  $L_y = 16$  (power-law decay discussed in [59]). Lower panel: correlations at  $J_3 = 0.8$  (long-range order). One sees an approximate period-10 modulation, corresponding to a wave vector  $2\pi \times \frac{3}{10} = 3\pi/5$ . The reference site for measuring the correlations is the fourth site ( $x = 4$ ) from the left boundary.

showing the development of spin order. In addition, we have also computed the spin correlation functions on a long strip  $12 \times 28$  for further check. In Fig. 8, the spin-spin correlations at  $J_3 = 0.35$  (in the gapless QSL phase),  $J_3 = 0.45$  and  $0.5$  (in the VBS phase), and  $J_3 = 0.8$  (spiral phase) are shown. In contrast to a power law decay at  $J_3 = 0.35$  (see more results in our other paper Ref. [62]), the spin correlations at  $J_3 = 0.5$  show a clear exponential decay with oscillations. Note at  $J_3 = 0.45$  and  $0.5$ , correlators  $(-1)^r \langle S_0 \cdot S_r \rangle$  have positive and negative values [74]. This is a signature of short-range spiral order (although with a very short correlation length) while, in the long-range spiral ordered phase, the spin correlations oscillate but saturate to a finite value at long distance.

To visualize the spin pattern, we compute the values of  $\langle S_{i_x, i_y}^x \rangle$ ,  $\langle S_{i_x, i_y}^y \rangle$  and  $\langle S_{i_x, i_y}^z \rangle$  on each site at  $J_3=0.8$  (set  $J_1 = 1$ ) and  $J_3/J_1 \rightarrow \infty$  (set  $J_1 = 0$ ). In Fig. 9(a) and Fig. 10(a) and (b),  $\langle S_{i_x, i_y}^z \rangle$  on each site are presented. At  $J_3 = 0.8$  we see clear indications of incommensurate long-range spiral order while for  $J_3/J_1 \rightarrow \infty$  it is commensurate with a period of 4 lattice spacings along both  $x$  and  $y$  directions, the 3rd-neighbour

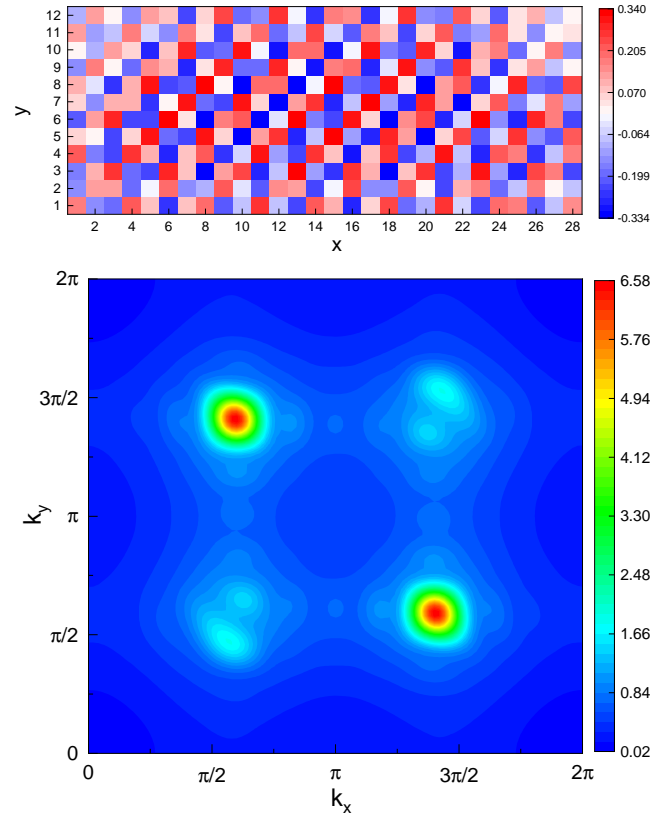


Figure 9. Spin pattern on a  $12 \times 28$  strip at  $J_3 = 0.8$  ( $J_2 = 0$ ). Upper panel:  $\langle S_{i_x, i_y}^z \rangle$  distribution. Lower panel: Spin structure factor based on  $z$ -component spin correlations, i.e.,  $S^{zz}(\mathbf{k})$ . The peak positions are located at  $(q, -q)$  and  $(-q, q)$  where  $q \approx \frac{3}{5}\pi$ .

spin pairs being always antiparallel. The spiral orders can be more explicitly visualized by also considering the  $x$  and  $y$  spin components. We find that the magnitude of the  $y$ -components  $\langle S_{i_x, i_y}^y \rangle$  is extremely small, at least three orders smaller than  $\langle S_{i_x, i_y}^z \rangle$  or  $\langle S_{i_x, i_y}^x \rangle$  according to our resolution, indicating that the spiral is coplanar (see Fig. 10(c) and (d)). The incommensurate (commensurate) long-range spiral order is also revealed by magnetic Bragg peaks at two (four) incommensurate (commensurate) wave vectors, as shown in Fig. 7(g) and Fig. 9(b) (Fig. 7(h)).

## B. $J_2 \neq 0$

Based on the above results at  $J_2 = 0$ , we have a good understanding of the properties of the VBS phase and of the spiral orders. We turn now to the  $J_2 \neq 0$  case to investigate the whole phase diagram of the spin-1/2  $J_1$ - $J_2$ - $J_3$  model. First, we focus on two typical cases  $J_2 = 0.3$  and  $J_2 = 0.5$ . At fixed  $J_2 = 0.3$ , increasing  $J_3$  from 0, the system sequentially experiences a AFM phase and a gapless QSL phase, and then enters the VBS phase. Note that for  $J_2 = 0.5$  there is no AFM phase for  $J_3 \geq 0$ . In both cases, when  $J_3$  is very large, the system lies in the long-range spiral ordered phase. Here

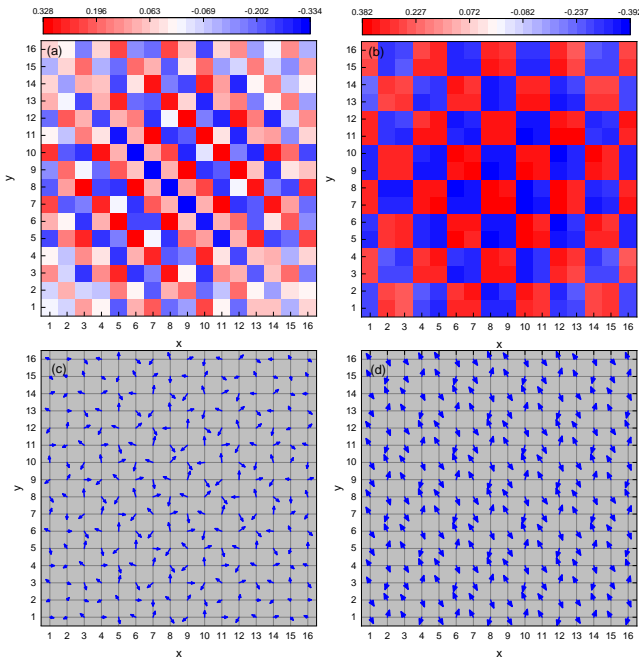


Figure 10. Spin patterns in the  $J_1$ - $J_3$  model on a  $16 \times 16$  open boundary system at  $J_3/J_1 = 0.8$  (a,c), and at  $J_3/J_1 \rightarrow \infty$  (b,d). (a,b) show the values of  $\langle S_{ix,iy}^z \rangle$ . (c,d) show the  $\langle \vec{S}_{ix,iy} \rangle$  vectors on each site in the  $(x, z)$  plane, drawn as  $(1.5 * \langle S_{ix,iy}^x \rangle, 1.5 * \langle S_{ix,iy}^z \rangle)$  in the  $(x, y)$  coordinate space.

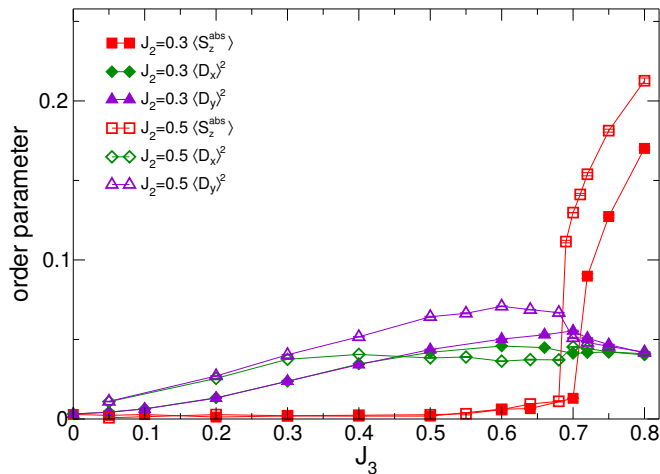


Figure 11.  $J_3$  dependence of the spin and dimer order parameters at fixed  $J_2 = 0.3$  and  $J_2 = 0.5$  values on  $12 \times 12$  sites. For both cases  $\langle S_z^{\text{AFM}} \rangle \simeq 0$  (not shown).

we compute the physical quantities on  $12 \times 12$  sites to check whether there exist other possible phases between the VBS and the spiral phase.

In Fig. 11, we present the variation of the spin and dimer order parameters with increasing  $J_3$ . We note that at  $J_2 = 0.3$  and  $J_3 = 0$  (in the AFM phase) the AFM order parameter  $\langle S_z^{\text{AFM}} \rangle$  on  $12 \times 12$  sites is still zero, in contrast to the results on  $16 \times 16$  sites at  $J_2 = 0$ . This is because  $L = 12$  is

still a bit too small to observe the spontaneous breaking of the  $SU(2)$  symmetry occurring in the AFM phase. Using  $L = 16$ , we observe similar results as in the  $J_2 = 0$  case (not shown). The other spin order parameter  $\langle S_z^{\text{abs}} \rangle$  shows a sharp change around  $J_3 = 0.7$  for both  $J_2 = 0.3$  and  $J_2 = 0.5$ , indicating a first-order transition into the long-range spiral ordered phase. In addition, the dimer order parameters  $\langle D_x \rangle^2$  and  $\langle D_y \rangle^2$  start to deviate from each other when  $J_3$  is large enough, and then have sudden changes at the first-order transitions. We have also checked the evolution of the spin structure factor with respect to  $J_3$ , as shown in Fig. 12, and found that the maximum of the spin structure factor gradually moves away from  $(\pi, \pi)$ . A comparison to the results obtained at  $J_2 = 0$  reveals similar features for the spin and dimer order parameters as well as for the spin structure factors, indicating there are no other phases between the VBS and spiral phases. Interestingly, as discussed above, the emergence of short-range spiral order seen in some region of the plaquette VBS phase may be seen as a precursor of the transitions to the mixed VBS phase and to the spiral phase (see transition lines reported in Fig. 1). We point out that, in contrast to the classical case showing the existence of a spiral phase ordered at wave vector  $(\pi, \pm q)$  or  $(\pm q, \pi)$ , both our PEPS and previous ED results do not support in the quantum spin-1/2 model such a long-range ordered spiral phase.

The phase diagram of the  $J_1$ - $J_2$ - $J_3$  model is becoming more precise now: we know it must contain the AFM, gapless QSL, VBS, stripe, long-range spiral order phases, as well as a unit-cell-enlarged AFM phase ordered at  $(\pm\pi/2, \pm\pi/2)$ . Since the VBS-spiral and VBS-stripe phase transitions are first-order, we can also use the exact ground state energies on a  $4 \times 4$  periodic system to evaluate the phase boundaries, see Fig. 16 in Appendix. B. We also use the PEPS results on larger open  $12 \times 12$  or  $16 \times 16$  systems to evaluate the VBS-spiral transition points for several  $(J_2, J_3)$  values, showing agreement with the corresponding estimations from the periodic  $4 \times 4$  cluster. The estimated phase boundaries can be seen in Fig. 1.

### C. AFM-spiral transition

It has been already shown in our previous work that for negative  $J_2 \lesssim -0.25$ , there exists a AFM-VBS transition line [62]. However, we find for a large negative  $J_2$  like  $J_2 = -1.2$ , the VBS phase disappears and a direct first order AFM-spiral phase transition occurs.

We first consider intermediate negative  $J_2$  values, say  $J_2 = -0.8$  or  $J_2 = -1.0$ . In this case, for a given  $J_2$ , increasing  $J_3$  leads to a continuous AFM-VBS transition followed by a first-order VBS-spiral transition. As discussed in Sec. II A 3, the VBS-spiral transition point can be generically determined by comparing energies with different initial states. In Fig. 13(a) and (b), we show the energy variation with respect to  $J_3$  when a VBS-spiral transition occurs on  $16 \times 16$ , at fixed  $J_2 = -0.8$  and  $J_2 = -1.0$  respectively. The AFM-VBS transition point can be evaluated by finite size scaling of the respective order parameters. In Fig. 13(c) and (d), we present the scaling of the AFM order parameter  $\langle M_0^2 \rangle$  and of the VBS order parameters

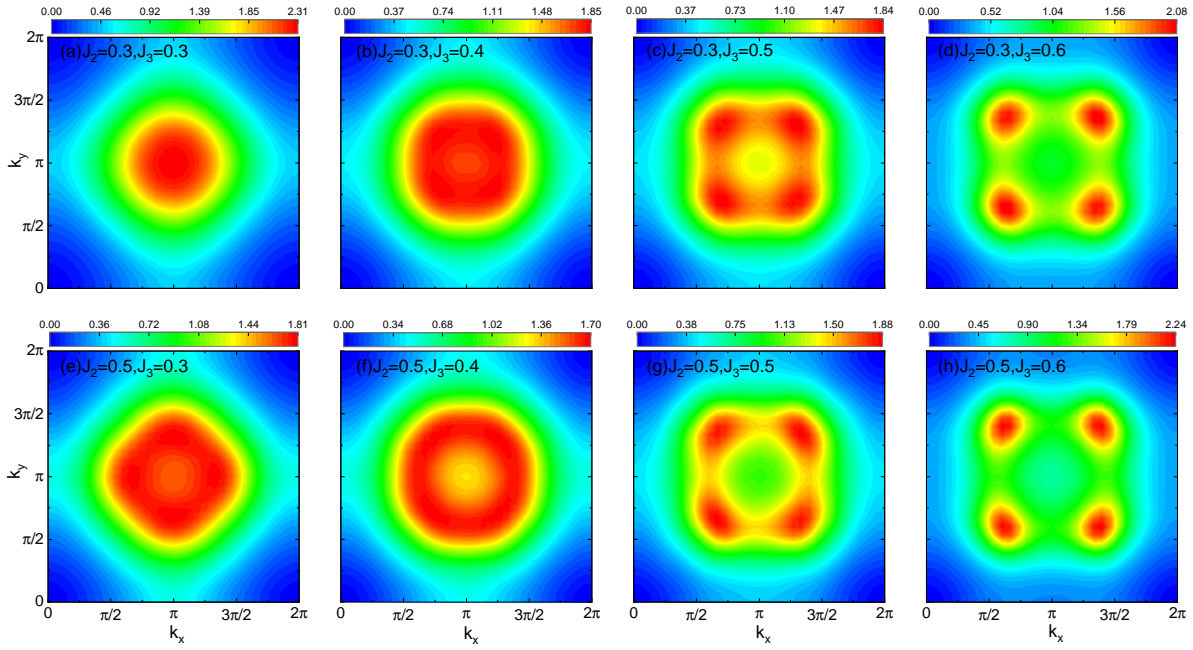


Figure 12. Spin structure factor on  $12 \times 12$  sites for increasing  $J_3$  using fixed  $J_2 = 0.3$  (a-d), and  $J_2 = 0.5$  (e-h) parameters. All these points are in the VBS phase. (c,d) and (f-h) correspond to the mixed columnar-plaquette VBS phase.

$\langle D \rangle^2 = \langle D_x \rangle^2 + \langle D_y \rangle^2$  for  $J_2 = -1.0$  as an example, where  $\langle M_0^z \rangle = \frac{1}{L^2} S(\mathbf{k}_0)$  and  $\mathbf{k}_0 = (\pi, \pi)$ . We find that the VBS phase is located in the interval  $0.92 \lesssim J_3 \lesssim 0.99$  at  $J_2 = -1.0$ . Upon increasing further the magnitude of (negative)  $J_2$ , the extension of the VBS region with  $J_3$  shrinks rapidly, leading to an end point of the continuous AFM-VBS transition.

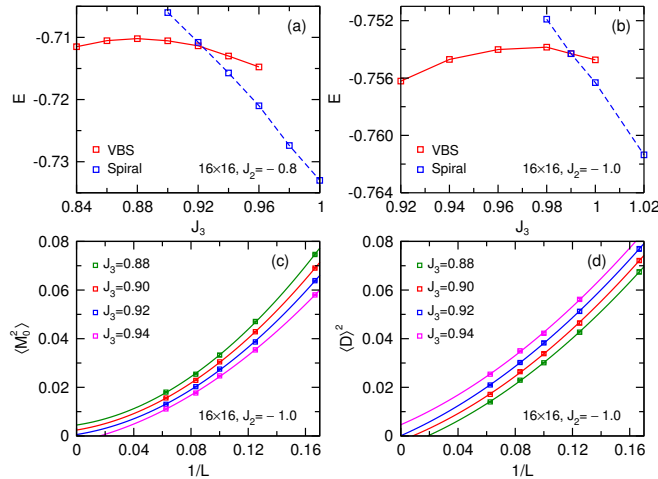


Figure 13. Energy as a function of  $J_3$  on  $16 \times 16$  at fixed  $J_2 = -0.8$  (a) and  $J_2 = -1.0$  (b). Red and blue symbols denote energies initialized by VBS and spiral states. (c-d) Finite size scaling of the AFM order parameter  $\langle M_0^z \rangle$  and the VBS order parameter  $\langle D \rangle^2$  at different  $J_3$  for a fixed  $J_2 = -1.0$ .

Now we turn to  $J_2 = -1.2$ , at which we find a direct first-order AFM-spiral transition with increasing  $J_3$ . Shown in Fig. 14, we can see there is a transition at  $J_3 \approx 1.06$ .

Actually, at  $J_3 = 1.06$ , the optimal AFM state has an energy  $E = -0.79285$ , very close to the optimal spiral state energy  $E = -0.79342$ , but they have apparent AFM and spiral spin patterns correspondingly (not shown). The ground state spin order parameters show sharp changes around  $J_3 = 1.06$  in Fig. 14(b), providing strong evidence for a first-order phase transition.

#### D. $J_3 < 0$

To get the complete phase diagram, we finally consider the region at negative  $J_3$ . For  $J_3 = 0$ , i.e. the  $J_1$ - $J_2$  model, a gapless QSL and a VBS phase emerge in between the AFM and stripe phases. A negative  $J_3$  enhances spin orders like the AFM and the stripe orders, and therefore destabilizes the QSL and VBS phases. Here we try to estimate how large a (negative)  $J_3$  should be to suppress the QSL and VBS phases.

We first consider a relatively large negative  $J_3$  value,  $J_3 = -0.1$ . In this case, we find a direct first-order transition between the AFM and stripe phases. At  $J_2 = 0.50$ , we observe a clear AFM pattern and the averaged local  $\langle S_{i_x, i_y}^z \rangle$  is about 0.026 on  $16 \times 16$ . Increasing  $J_2$  to 0.58, this value is reduced to 0.016, still showing a clear AFM order. Meanwhile, the local dimer order  $\langle D \rangle^2 = \langle D_x \rangle^2 + \langle D_y \rangle^2$  remains much smaller, about 0.0067. The AFM-stripe is a typical first-order transition, and the  $J_2$  transition point is expected to shift as the system size increases, similarly to the VBS-stripe transition in the  $J_1$ - $J_2$  model [59]. As discussed in Sec. II A 3, we can evaluate the transition point by starting the PEPS optimization either from an AFM state or from a stripe state. Using the crossing of the energy curves shown in Fig. 15(a), the transition points

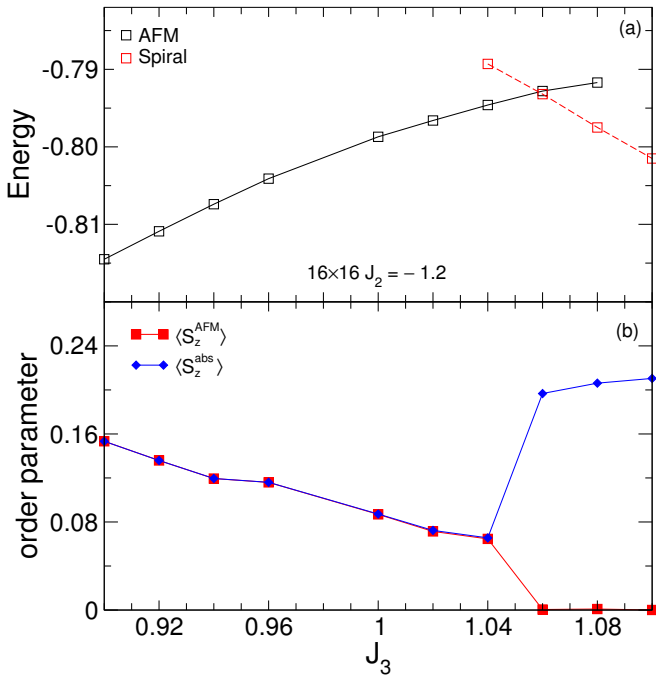


Figure 14. Energy and spin order parameters versus  $J_3$  on  $16 \times 16$  at fixed  $J_2 = -1.2$ . (a) Black and red symbols denote the optimal AFM energies and optimal spiral energies, respectively. (b) The variation of the ground state spin order parameters.

$J_2^c(L)$  can be obtained  $-0.656$ ,  $0.630$  and  $0.618$  for  $8 \times 8$ ,  $12 \times 12$  and  $16 \times 16$ , respectively – and reported in Fig. 15(b). Next, the first-order transition point in the thermodynamic limit can be evaluated by a linear extrapolation in  $1/L$  giving  $J_2^c(L \rightarrow \infty) = 0.58$ . As the bulk energy on  $16 \times 16$  sites can better approximate the energy in the thermodynamic limit, following Ref. [59], we also use the central  $4 \times 4$  bulk energy of the  $16 \times 16$  open system to estimate the thermodynamic limit transition point, which gives a consistent value  $J_2^c(L \rightarrow \infty) \approx 0.582$ . The study of the spin and dimer local order parameters shown in Fig. 15(c) also confirms the first-order transition.

We further consider a smaller interaction of  $J_3$ , say,  $J_3 = -0.05$ . Still using  $J_2 = 0.58$ , we find the spin order  $\langle S_{i_x, i_y}^z \rangle$  at  $(J_2, J_3) = (0.58, -0.05)$  is  $0.008$ , half the value obtained at  $(J_2, J_3) = (0.58, -0.1)$ . This means  $(J_2, J_3) = (0.58, -0.05)$  could still be in the AFM phase, but rather close to the nonmagnetic phase. These results indicate that both the gapless QSL and VBS phases may disappear for a quite small negative value of  $J_3$ . In such a narrow region, it is hard to determine accurately the transition lines of the QSL and VBS phases. We schematically show in the inset of Fig. 1 the phase boundaries of the QSL and VBS phases for  $J_3 < 0$  ending in two multicritical points. Here we assume the gapless QSL does not touch the stripe phase which remains separated by the VBS phase. We believe a first-order transition always occurs between the stripe phase and other phases, in that case the AFM and VBS phases. As the two putative multicritical points are very close, another scenario is that the AFM, QSL, VBS and stripe phases are directly connected by a quadruple

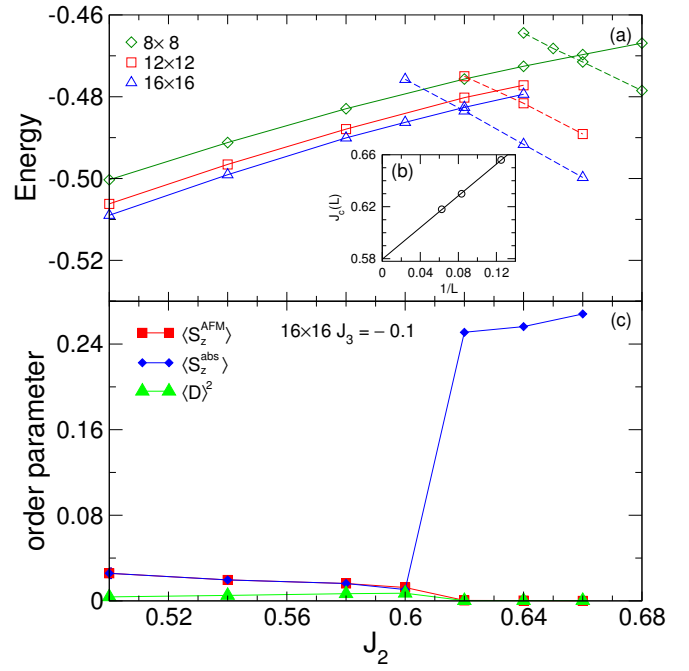


Figure 15. (a) Energy dependence versus  $J_2$  on  $8 \times 8$ ,  $12 \times 12$  and  $16 \times 16$  open systems at fixed  $J_3 = -0.1$ . The dashed lines denote the energies using the stripe state as an initialization. (b) The first-order transition point  $J_2^c(L \rightarrow \infty)$  evaluated in the thermodynamic limit from a linear extrapolation in  $1/L$  of the transition points  $J_2^c(L)$ . (c) The spin and dimer local order parameters on  $16 \times 16$  at different  $J_2$  with fixed  $J_3 = -0.1$ .

point.

### III. CONCLUSION AND DISCUSSION

In this work, we establish the global phase diagram of the  $J_1$ - $J_2$ - $J_3$  model using finite PEPS algorithms with careful finite size scaling. We compute the spin and dimer order parameters, as well as the spin-spin correlation functions. First, we focus on the properties of the VBS phase and find a novel transition from the 4-fold degenerate plaquette VBS phase (beyond the boundary with the previously discovered QSL phase) to a 8-fold degenerate mixed-VBS phase (e.g. in the  $J_1$ - $J_3$  model increasing  $J_3$ ). The later VBS phase can be viewed as spontaneously breaking the point group  $C_4$ -symmetry of the plaquette VBS. In other words, while in the plaquette VBS phase horizontal and vertical dimers have the same magnitude, they become gradually different at the transition to the mixed-VBS. The mixed-VBS phase shows also interesting incommensurate short-range spin correlations while approaching the magnetic spiral phase ordered at wave vectors  $(\pm q, \pm q)$ . Our results combined with previous studies suggest that the transition between the plaquette and the mixed columnar-plaquette VBS phases is continuous as expected from Ginzburg-Landau paradigm and studies of quantum dimer models [71]. In contrast, the transition between the mixed-VBS and the spiral phase is found to be first-order.

In the latter spiral phase, we clearly establish the existence of long-range spiral spin correlations, and explicitly visualize incommensurate spiral patterns in real space.

Therefore, the overall ground state phase diagram of the  $J_1$ - $J_2$ - $J_3$  model is elucidated in detail, containing six phases: an AFM phase ordered at  $(\pi, \pi)$ , a stripe phase ordered at  $(\pi, 0)$  or  $(0, \pi)$ , two VBS phases, a gapless QSL phase, a spiral phase ordered at  $(\pm q, \pm q)$  (including the phase ordered at  $(\pm\pi/2, \pm\pi/2)$ ). We would like to stress that our work significantly broadens the knowledge on VBS and spiral orders. It also provides a canonical example for the understanding of quantum effects and competition caused by frustration, the spin-1/2  $J_1$ - $J_2$ - $J_3$  model showing a large paramagnetic region in which exotic phases develop. Interestingly, we find that the QSL and VBS phases of the  $J_1$ - $J_2$  model, easily suppressed by a very small negative  $J_3 = -0.02 \sim -0.05$ , are rather close to the multicritical points occurring at quite small  $J_3 < 0$  as seen in Fig. 1. This naturally explains the very long correlation lengths found in the previous studies of the pure  $J_1$ - $J_2$  model [47, 52, 59].

Furthermore, We find two distinct types of multicritical points within the complete phase diagram. The first type involves critical points at which three continuous transition lines intersect: AFM-VBS, AFM-QSL, and QSL-VBS (two blue dots in Fig. 1). The second type encompasses critical points that mark the termination of a continuous line culminating in a first-order transition, which occurs with the AFM-VBS critical line reaching either the spiral phase or the stripe (two red dots in Fig. 1). It is noteworthy that these two types of critical points are conceptually different. Intriguingly, the continuous AFM-VBS transition, functioning as a line of deconfined quantum critical points (DQCP) [62], can culminate at both types of multicritical points. This observation could offer valuable insights into comprehending the nature of the DQCP [61, 75]. Our results are also helpful for experimental investigation on square-lattice frustrated magnets.

Finally, we would like to point out that our study further demonstrates the capability of finite PEPS as a powerful numerical tool to study strongly-correlated 2D quantum many-body systems. Tensor elements of finite PEPS can be independent, and thus finite PEPS constitutes a very general ansatz family and can naturally capture nonuniform properties. In particular, the power of finite PEPS has been fully explored when it is used to accurately represent incommensurate short-range or long-range orders. We note that in fermionic correlated models like the  $t$ - $J$  model, short-range incommensurate correlations can also exist [3], and hence finite PEPS method could be able to provide accurate results.

#### IV. ACKNOWLEDGMENT

We thank Gang Chen, Zheng-Xin Liu, Han-Qiang Wu and Rong Yu for helpful discussions. This work is supported by the CRF C7012-21GF, the ANR/RGC Joint Research Scheme No. A-CUHK402/18 from the Hong Kong's Research Grants Council and the TNTOP ANR-18-

CE30-0026-01 grants awarded from the French Research Council. Wei-Qiang Chen is supported by the National Key R&D Program of China (Grants No. 2022YFA1403700), NSFC (Grants No. 12141402), the Science, Technology and Innovation Commission of Shenzhen Municipality (No. ZDSYS20190902092905285), Guangdong Basic and Applied Basic Research Foundation under Grant No. 2020B1515120100, and Center for Computational Science and Engineering at Southern University of Science and Technology. S.S.G. was supported by the NSFC Grants No. 11874078 and No. 11834014.

#### Appendix A: convergence with $D$

Here we check the  $D$ -convergence on a  $16 \times 16$  open system at  $(J_2, J_3) = (-1, 0.8)$ . In Table I, we present the obtained  $D = 4 - 10$  results for energy, dimerization and magnetization. It clearly indicates  $D = 8$  is sufficient to get converged results.

Table I. The convergence of physical quantities with respect to the PEPS bond dimension  $D$  on a  $16 \times 16$  system at  $(J_2, J_3) = (-1, 0.8)$ , including ground state energy per site, dimerization  $\langle D \rangle^2 = \langle D_x \rangle^2 + \langle D_y \rangle^2$ , and AFM magnetization  $\langle M_z^2 \rangle = \langle (S_z^{\text{AFM}})^2 \rangle$  (see main text for detailed definitions).

$D$	$E$	$\langle D \rangle^2$	$\langle M_z^2 \rangle$
4	-0.769042(6)	0.00656(9)	0.0290(1)
6	-0.772245(4)	0.00686(8)	0.0261(2)
8	-0.773084(3)	0.00701(6)	0.0217(1)
10	-0.773092(5)	0.00701(8)	0.0218(2)

#### Appendix B: $4 \times 4$ results from exact diagonalization

As the VBS-spiral and VBS-stripe phase transitions are first-order, we use the exact ground state energies on a  $4 \times 4$  periodic system to estimate the phase boundaries, as shown in Fig. 16. For the VBS-stripe transition, given  $J_3 = 0$ , we have found that the transition point is located at  $J_2 = 0.61$  [59]. Here the second derivative of the  $4 \times 4$  energy with respect to  $J_2$  gives an estimate of the transition point around  $J_2 = 0.626$ , in good agreement. For the VBS-spiral transition at fixed  $J_2 = 0, 0.3$  and  $0.5$ , the transition points obtained by PEPS calculations on open  $16 \times 16$  or  $12 \times 12$  systems, are  $J_3 \simeq 0.75, 0.70$  and  $0.68$ , respectively, also consistent with the corresponding estimations from the periodic  $4 \times 4$  cluster, namely  $J_3 \simeq 0.757, 0.691$  and  $0.674$ .

#### Appendix C: spin structure factor in mixed-VBS phase

We have shown the contour plots of the spin structure factor  $S(\mathbf{k})$  of the  $J_1$ - $J_3$  model in Fig. 5. Here we have a much closer look at  $S(\mathbf{k})$  in the mixed-VBS phase searching for (weak) signatures of the spontaneously breaking of the  $\pi/2$  rotation

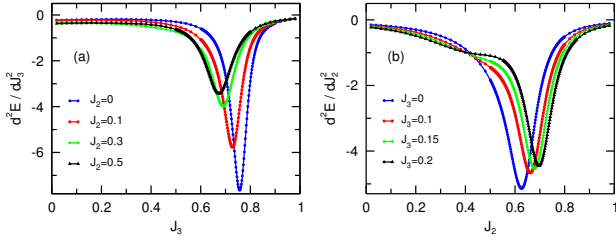


Figure 16. (a) Second derivative of the ground state energy with respect to  $J_3$  for given  $J_2$  values on a periodic  $4 \times 4$  system to estimate the VBS-spiral phase transition point. (b) Second derivative of the ground state energy with respect to  $J_2$  for given  $J_3$  values on a periodic  $4 \times 4$  system to estimate the VBS-stripe phase transition point.

symmetry. In Fig. 17, we present  $S(\mathbf{k})$  along  $k_x = k_y$  and  $k_x = -k_y$  at  $J_3 = 0.5$  (inside the plaquette VBS phase) and  $J_3 = 0.7$  (inside the mixed columnar-plaquette VBS phase).

At  $J_3 = 0.5$ , the two curves are almost identical, consistent with a  $\pi/2$  rotation symmetry for the plaquette VBS. In contrast, at  $J_3 = 0.7$ , they show visible differences around the maxima, indicating the breaking of  $\pi/2$  rotation symmetry in the mixed VBS phase. Note that a clear incommensurability and a larger spin correlation length (estimated from the inverse of the width of the peaks) are seen in this case.

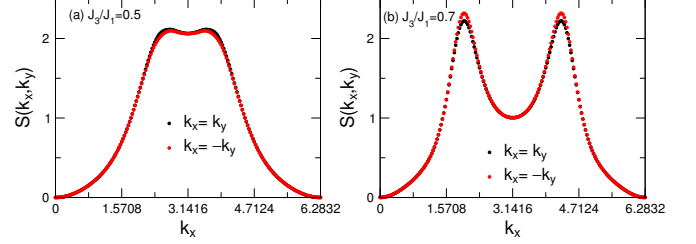


Figure 17. Spin structure factor in the  $J_1$ - $J_3$  model at  $J_3 = 0.5$  and  $0.7$  on  $16 \times 16$ , along  $k_x = k_y$  and  $k_x = -k_y$ .

- [1] P. W. Anderson, “The resonating valence bond state in  $\text{La}_2\text{CuO}_4$  and superconductivity,” *Science* **235**, 1196–1198 (1987).
- [2] Martin P. Gelfand, Rajiv R. P. Singh, and David A. Huse, “Zero-temperature ordering in two-dimensional frustrated quantum Heisenberg antiferromagnets,” *Phys. Rev. B* **40**, 10801–10809 (1989).
- [3] Adriana Moreo, Elbio Dagotto, Thierry Jolicoeur, and José Riera, “Incommensurate correlations in the  $t$ - $J$  and frustrated spin-1/2 Heisenberg models,” *Phys. Rev. B* **42**, 6283–6293 (1990).
- [4] P. Chandra and B. Douçot, “Possible spin-liquid state at large  $S$  for the frustrated square Heisenberg lattice,” *Phys. Rev. B* **38**, 9335–9338 (1988).
- [5] F. Figueirido, A. Karlhede, S. Kivelson, S. Sondhi, M. Rocek, and D. S. Rokhsar, “Exact diagonalization of finite frustrated spin-1/2 Heisenberg models,” *Phys. Rev. B* **41**, 4619–4632 (1990).
- [6] Andrey Chubukov, “First-order transition in frustrated quantum antiferromagnets,” *Phys. Rev. B* **44**, 392–394 (1991).
- [7] N. Read and Subir Sachdev, “Large- $N$  expansion for frustrated quantum antiferromagnets,” *Phys. Rev. Lett.* **66**, 1773–1776 (1991).
- [8] L. B. Ioffe and A. I. Larkin, “Effective action of a two-dimensional antiferromagnet,” *Int. J. Mod. Phys. B* **2**, 203–219 (1988).
- [9] Torbjörn Einarsson and Henrik Johannesson, “Effective-action approach to the frustrated Heisenberg antiferromagnet in two dimensions,” *Phys. Rev. B* **43**, 5867–5882 (1991).
- [10] Jaime Ferrer, “Spin-liquid phase for the frustrated quantum Heisenberg antiferromagnet on a square lattice,” *Phys. Rev. B* **47**, 8769–8782 (1993).
- [11] Luca Capriotti and Subir Sachdev, “Low-temperature broken-symmetry phases of spiral antiferromagnets,” *Phys. Rev. Lett.* **93**, 257206 (2004).
- [12] P. W. Leung and Ngar-wing Lam, “Numerical evidence for the spin-Peierls state in the frustrated quantum antiferromagnet,” *Phys. Rev. B* **53**, 2213–2216 (1996).
- [13] Luca Capriotti, Douglas J. Scalapino, and Steven R. White, “Spin-liquid versus dimerized ground states in a frustrated Heisenberg antiferromagnet,” *Phys. Rev. Lett.* **93**, 177004 (2004).
- [14] Matthieu Mambrini, Andreas Läuchli, Didier Poilblanc, and Frédéric Mila, “Plaquette valence-bond crystal in the frustrated Heisenberg quantum antiferromagnet on the square lattice,” *Phys. Rev. B* **74**, 144422 (2006).
- [15] A. Ralko, M. Mambrini, and D. Poilblanc, “Generalized quantum dimer model applied to the frustrated Heisenberg model on the square lattice: Emergence of a mixed columnar-plaquette phase,” *Phys. Rev. B* **80**, 184427 (2009).
- [16] M. S. L. du Croo de Jongh, J. M. J. van Leeuwen, and W. van Saarloos, “Incorporation of density-matrix wave functions in monte carlo simulations: Application to the frustrated Heisenberg model,” *Phys. Rev. B* **62**, 14844–14854 (2000).
- [17] Philippe Sindzingre, Nic Shannon, and Tsutomu Momoi, “Phase diagram of the spin-1/2  $J_1$ - $J_2$ - $J_3$  Heisenberg model on the square lattice,” *Journal of Physics: Conference Series* **200**, 022058 (2010).
- [18] Elbio Dagotto and Adriana Moreo, “Phase diagram of the frustrated spin-1/2 Heisenberg antiferromagnet in 2 dimensions,” *Phys. Rev. Lett.* **63**, 2148–2151 (1989).
- [19] Subir Sachdev and R. N. Bhatt, “Bond-operator representation of quantum spins: Mean-field theory of frustrated quantum Heisenberg antiferromagnets,” *Phys. Rev. B* **41**, 9323–9329 (1990).
- [20] Didier Poilblanc, Eduardo Gagliano, Silvia Bacci, and Elbio Dagotto, “Static and dynamical correlations in a spin-1/2 frustrated antiferromagnet,” *Phys. Rev. B* **43**, 10970–10983 (1991).
- [21] Andrey V. Chubukov and Th. Jolicoeur, “Dimer stability region in a frustrated quantum Heisenberg antiferromagnet,” *Phys. Rev. B* **44**, 12050–12053 (1991).
- [22] H. J. Schulz and T. A. L. Ziman, “Finite-size scaling for the two-dimensional frustrated quantum Heisenberg antiferromagnet,” *Europhysics Letters* **18**, 355–360 (1992).

- [23] N. B. Ivanov and P. Ch. Ivanov, “Frustrated two-dimensional quantum Heisenberg antiferromagnet at low temperatures,” *Phys. Rev. B* **46**, 8206–8213 (1992).
- [24] T. Einarsson and H. J. Schulz, “Direct calculation of the spin stiffness in the  $J_1$ - $J_2$  Heisenberg antiferromagnet,” *Phys. Rev. B* **51**, 6151–6154 (1995).
- [25] T. A. L. Ziman H. J. Schulz and D. Poilblanc, “Magnetic order and disorder in the frustrated quantum Heisenberg antiferromagnet in two dimensions,” *J. Phys. I* **6**, 675–703 (1996).
- [26] M. E. Zhitomirsky and Kazuo Ueda, “Valence-bond crystal phase of a frustrated spin-1/2 square-lattice antiferromagnet,” *Phys. Rev. B* **54**, 9007–9010 (1996).
- [27] Rajiv R. P. Singh, Zheng Weihong, C. J. Hamer, and J. Oitmaa, “Dimer order with striped correlations in the  $J_1$ - $J_2$  Heisenberg model,” *Phys. Rev. B* **60**, 7278–7283 (1999).
- [28] Luca Capriotti and Sandro Sorella, “Spontaneous plaquette dimerization in the  $J_1$ - $J_2$  Heisenberg model,” *Phys. Rev. Lett.* **84**, 3173–3176 (2000).
- [29] Luca Capriotti, Federico Becca, Alberto Parola, and Sandro Sorella, “Resonating valence bond wave functions for strongly frustrated spin systems,” *Phys. Rev. Lett.* **87**, 097201 (2001).
- [30] Guang-Ming Zhang, Hui Hu, and Lu Yu, “Valence-bond spin-liquid state in two-dimensional frustrated spin-1/2 Heisenberg antiferromagnets,” *Phys. Rev. Lett.* **91**, 067201 (2003).
- [31] Ken’ichi Takano, Yoshiya Kito, Yoshiaki Ōno, and Kazuhiro Sano, “Nonlinear  $\sigma$  model method for the  $J_1$ - $J_2$  Heisenberg model: Disordered ground state with plaquette symmetry,” *Phys. Rev. Lett.* **91**, 197202 (2003).
- [32] J. Sirker, Zheng Weihong, O. P. Sushkov, and J. Oitmaa, “ $J_1$ - $J_2$  model: First-order phase transition versus deconfinement of spinons,” *Phys. Rev. B* **73**, 184420 (2006).
- [33] D. Schmalfuß, R. Darradi, J. Richter, J. Schulenburg, and D. Ihle, “Quantum  $J_1$ - $J_2$  antiferromagnet on a stacked square lattice: Influence of the interlayer coupling on the ground-state magnetic ordering,” *Phys. Rev. Lett.* **97**, 157201 (2006).
- [34] R. Darradi, O. Derzhko, R. Zinke, J. Schulenburg, S. E. Krüger, and J. Richter, “Ground state phases of the spin-1/2  $J_1$ - $J_2$  Heisenberg antiferromagnet on the square lattice: A high-order coupled cluster treatment,” *Phys. Rev. B* **78**, 214415 (2008).
- [35] Marcelo Arlego and Wolfram Brenig, “Plaquette order in the  $J_1$ - $J_2$ - $J_3$  model: Series expansion analysis,” *Phys. Rev. B* **78**, 224415 (2008).
- [36] L. Isaev, G. Ortiz, and J. Dukelsky, “Hierarchical mean-field approach to the  $J_1$ - $J_2$  Heisenberg model on a square lattice,” *Phys. Rev. B* **79**, 024409 (2009).
- [37] V. Murg, F. Verstraete, and J. I. Cirac, “Exploring frustrated spin systems using projected entangled pair states,” *Phys. Rev. B* **79**, 195119 (2009).
- [38] K. S. D. Beach, “Master equation approach to computing rvb bond amplitudes,” *Phys. Rev. B* **79**, 224431 (2009).
- [39] J. Richter and J. Schulenburg, “The spin-1/2  $J_1$ - $J_2$  Heisenberg antiferromagnet on the square lattice: Exact diagonalization for  $N = 40$  spins,” *The European Physical Journal B* **73**, 117 (2010).
- [40] Ji-Feng Yu and Ying-Jer Kao, “Spin- $\frac{1}{2}$   $J_1$ - $J_2$  Heisenberg antiferromagnet on a square lattice: A plaquette renormalized tensor network study,” *Phys. Rev. B* **85**, 094407 (2012).
- [41] Hong-Chen Jiang, Hong Yao, and Leon Balents, “Spin liquid ground state of the spin- $\frac{1}{2}$  square  $J_1$ - $J_2$  Heisenberg model,” *Phys. Rev. B* **86**, 024424 (2012).
- [42] Fabio Mezzacapo, “Ground-state phase diagram of the quantum  $J_1$ - $J_2$  model on the square lattice,” *Phys. Rev. B* **86**, 045115 (2012).
- [43] Ling Wang, Didier Poilblanc, Zheng-Cheng Gu, Xiao-Gang Wen, and Frank Verstraete, “Constructing a gapless spin-liquid state for the spin-1/2  $J_1$ - $J_2$  Heisenberg model on a square lattice,” *Phys. Rev. Lett.* **111**, 037202 (2013).
- [44] Wen-Jun Hu, Federico Becca, Alberto Parola, and Sandro Sorella, “Direct evidence for a gapless  $Z_2$  spin liquid by frustrating néel antiferromagnetism,” *Phys. Rev. B* **88**, 060402 (2013).
- [45] R. L. Doretto, “Plaquette valence-bond solid in the square-lattice  $J_1$ - $J_2$  antiferromagnet Heisenberg model: A bond operator approach,” *Phys. Rev. B* **89**, 104415 (2014).
- [46] Yang Qi and Zheng-Cheng Gu, “Continuous phase transition from Néel state to  $Z_2$  spin-liquid state on a square lattice,” *Phys. Rev. B* **89**, 235122 (2014).
- [47] Shou-Shu Gong, Wei Zhu, D. N. Sheng, Olexei I. Motrunich, and Matthew P. A. Fisher, “Plaquette ordered phase and quantum phase diagram in the spin- $\frac{1}{2}$   $J_1$ - $J_2$  square Heisenberg model,” *Phys. Rev. Lett.* **113**, 027201 (2014).
- [48] Chung-Pin Chou and Hong-Yi Chen, “Simulating a two-dimensional frustrated spin system with fermionic resonating-valence-bond states,” *Phys. Rev. B* **90**, 041106 (2014).
- [49] Satoshi Morita, Ryui Kaneko, and Masatoshi Imada, “Quantum spin liquid in spin 1/2  $J_1$ - $J_2$  Heisenberg model on square lattice: Many-variable variational monte carlo study combined with quantum-number projections,” *Journal of the Physical Society of Japan* **84**, 024720 (2015).
- [50] Johannes Richter, Ronald Zinke, and Damian J. J. Farnell, “The spin-1/2 square-lattice  $J_1$ - $J_2$  model: the spin-gap issue,” *The European Physical Journal B* **88**, 2 (2015).
- [51] Ling Wang, Zheng-Cheng Gu, Frank Verstraete, and Xiao-Gang Wen, “Tensor-product state approach to spin- $\frac{1}{2}$  square  $J_1$ - $J_2$  antiferromagnetic Heisenberg model: Evidence for deconfined quantum criticality,” *Phys. Rev. B* **94**, 075143 (2016).
- [52] Didier Poilblanc and Matthieu Mambrini, “Quantum critical phase with infinite projected entangled paired states,” *Phys. Rev. B* **96**, 014414 (2017).
- [53] Ling Wang and Anders W. Sandvik, “Critical level crossings and gapless spin liquid in the square-lattice spin-1/2  $J_1$ - $J_2$  Heisenberg antiferromagnet,” *Phys. Rev. Lett.* **121**, 107202 (2018).
- [54] R. Haghshenas and D. N. Sheng, “ $u(1)$ -symmetric infinite projected entangled-pair states study of the spin-1/2 square  $J_1$ - $J_2$  Heisenberg model,” *Phys. Rev. B* **97**, 174408 (2018).
- [55] Wen-Yuan Liu, Shaojun Dong, Chao Wang, Yongjian Han, Hong An, Guang-Can Guo, and Lixin He, “Gapless spin liquid ground state of the spin-1/2  $J_1$ - $J_2$  Heisenberg model on square lattices,” *Phys. Rev. B* **98**, 241109 (2018).
- [56] Didier Poilblanc, Matthieu Mambrini, and Sylvain Capponi, “Critical colored-RVB states in the frustrated quantum Heisenberg model on the square lattice,” *SciPost Phys.* **7**, 41 (2019).
- [57] Juraj Hasik, Didier Poilblanc, and Federico Becca, “Investigation of the néel phase of the frustrated Heisenberg antiferromagnet by differentiable symmetric tensor networks,” *SciPost Phys.* **10**, 12 (2021).
- [58] Francesco Ferrari and Federico Becca, “Gapless spin liquid and valence-bond solid in the  $J_1$ - $J_2$  Heisenberg model on the square lattice: Insights from singlet and triplet excitations,” *Phys. Rev. B* **102**, 014417 (2020).
- [59] Wen-Yuan Liu, Shou-Shu Gong, Yu-Bin Li, Didier Poilblanc, Wei-Qiang Chen, and Zheng-Cheng Gu, “Gapless quantum spin liquid and global phase diagram of the spin-1/2  $J_1$ - $J_2$  square antiferromagnetic Heisenberg model,” *Science Bulletin*

- 67, 1034–1041 (2022).
- [60] Yusuke Nomura and Masatoshi Imada, “Dirac-type nodal spin liquid revealed by refined quantum many-body solver using neural-network wave function, correlation ratio, and level spectroscopy,” *Phys. Rev. X* **11**, 031034 (2021).
- [61] T. Senthil, Ashvin Vishwanath, Leon Balents, Subir Sachdev, and Matthew P. A. Fisher, “Deconfined quantum critical points,” *Science* **303**, 1490–1494 (2004).
- [62] Wen-Yuan Liu, Juraj Hasik, Shou-Shu Gong, Didier Poilblanc, Wei-Qiang Chen, and Zheng-Cheng Gu, “Emergence of gapless quantum spin liquid from deconfined quantum critical point,” *Phys. Rev. X* **12**, 031039 (2022).
- [63] Muwei Wu, Shou-Shu Gong, Dao-Xin Yao, and Han-Qing Wu, “Phase diagram and magnetic excitations of  $J_1$ - $J_3$  Heisenberg model on the square lattice,” *Phys. Rev. B* **106**, 125129 (2022).
- [64] Philippe Corboz, Steven R. White, Guifré Vidal, and Matthias Troyer, “Stripes in the two-dimensional  $t$ - $J$  model with infinite projected entangled-pair states,” *Phys. Rev. B* **84**, 041108 (2011).
- [65] Philippe Corboz, T. M. Rice, and Matthias Troyer, “Competing states in the  $t$ - $J$  model: Uniform d-wave state versus stripe state,” *Phys. Rev. Lett.* **113**, 046402 (2014).
- [66] Bo-Xiao Zheng, Chia-Min Chung, Philippe Corboz, Georg Ehlers, Ming-Pu Qin, Reinhard M Noack, Hao Shi, Steven R White, Shiwei Zhang, and Garnet Kin-Lic Chan, “Stripe order in the underdoped region of the two-dimensional Hubbard model,” *Science* **358**, 1155–1160 (2017).
- [67] Wen-Yuan Liu, Shao-Jun Dong, Yong-Jian Han, Guang-Can Guo, and Lixin He, “Gradient optimization of finite projected entangled pair states,” *Phys. Rev. B* **95**, 195154 (2017).
- [68] Wen-Yuan Liu, Yi-Zhen Huang, Shou-Shu Gong, and Zheng-Cheng Gu, “Accurate simulation for finite projected entangled pair states in two dimensions,” *Phys. Rev. B* **103**, 235155 (2021).
- [69] Wen-Yuan Liu, Shou-Shu Gong, Wei-Qiang Chen, and Zheng-Cheng Gu, “Emergent symmetry in frustrated magnets: From deconfined quantum critical point to gapless quantum spin liquid,” [arXiv:2212.00707](https://arxiv.org/abs/2212.00707) (2022).
- [70] Wen-Yuan Liu, Xiao-Tian Zhang, Zhe Wang, Shou-Shu Gong, Wei-Qiang Chen, and Zheng-Cheng Gu, “Deconfined quantum criticality with emergent symmetry in the extended shastry-sutherland model,” [arXiv: 2309.10955](https://arxiv.org/abs/2309.10955) (2023).
- [71] A. Ralko, D. Poilblanc, and R. Moessner, “Generic mixed columnar-plaquette phases in Rokhsar-Kivelson models,” *Phys. Rev. Lett.* **100**, 037201 (2008).
- [72] H. C. Jiang, Z. Y. Weng, and T. Xiang, “Accurate determination of tensor network state of quantum lattice models in two dimensions,” *Phys. Rev. Lett.* **101**, 090603 (2008).
- [73] Peter Locher, “Linear spin waves in a frustrated Heisenberg model,” *Phys. Rev. B* **41**, 2537–2539 (1990).
- [74] There is a typo in Fig.4(a) in Ref. [62]; the y-axis label should read  $|\langle S_0 \cdot S_r \rangle|$ , rather than  $(-1)^r \langle S_0 \cdot S_r \rangle$ .
- [75] T. Senthil, Leon Balents, Subir Sachdev, Ashvin Vishwanath, and Matthew P. A. Fisher, “Quantum criticality beyond the Landau-Ginzburg-Wilson paradigm,” *Phys. Rev. B* **70**, 144407 (2004).